Geological Magazine

www.cambridge.org/geo

Origin of the Fule Pb–Zn deposit, Yunnan Province, SW China: insight from *in situ* S isotope analysis by NanoSIMS

Zhenli Li[1,2], Lin Ye[1], Yusi Hu[1,2], Zhilong Huang[1], Chen Wei[1,2] and Tao Wu[1,2]

[1]State Key Laboratory of Ore Deposit Geochemistry, Institute of Geochemistry, Chinese Academy of Sciences, Guiyang 550081, China and [2]University of Chinese Academy of Sciences, Beijing 100049, China

Original Article

Cite this article: Li Z, Ye L, Hu Y, Huang Z, Wei C, and Wu T (2020) Origin of the Fule Pb–Zn deposit, Yunnan Province, SW China: insight from *in situ* S isotope analysis by NanoSIMS. *Geological Magazine* **157**: 393–404. https://doi.org/10.1017/S0016756819000852

Received: 18 January 2019
Revised: 25 May 2019
Accepted: 14 June 2019
First published online: 30 October 2019

Keywords:
NanoSIMS; *in situ* S isotopic composition; sphalerite; pyrite; Fule Pb–Zn deposit

Author for correspondence:
Lin Ye, Email: yelin@vip.gyig.ac.cn

Abstract

The Sichuan–Yunnan–Guizhou (SYG) Pb–Zn metallogenic province is one of the most productive areas of Pb–Zn resources in China. The Fule deposit occurs in Permian carbonate and contains Pb–Zn reserves exceeding 1 Mt. To investigate the sulphur source, *in situ* S isotopic analysis of sphalerite and pyrite was carried out using nanoscale secondary-ion mass spectrometry. The results show that the $\delta^{34}S$ values of the sulphide minerals range from +16.1‰ to +23.0‰, higher than that of marine sulphates hosted in Permian carbonate rocks (+11‰), but similar to that of sulphates over a broader area (+12.9‰ to +25.9‰). The sulphates in the regional rocks could therefore represent an important source of S for the Fule deposit via thermochemical sulphate reduction. The S source of the Fule deposit is different from those of most other Pb–Zn deposits in the SYG Pb–Zn mineralization province, which were mainly derived from the ore-bearing strata. The $\delta^{34}S$ values of the early to late generations and some single sulphide crystals from the cores to rims show a slight increasing trend, implying that partial Rayleigh fractionation took place in the Fule deposit. It is suggested that the Fule sulphide precipitation resulted from the mixing of a metalliferous fluid with a H_2S-rich fluid derived from the regional strata. Combining the geology, mineralogy and S isotope results with previous Pb isotope studies, it is suggested that the Fule deposit should be attributed to a Mississippi Valley type deposit.

1. Introduction

The Sichuan–Yunnan–Guizhou (SYG) Pb–Zn metallogenic province (Fig. 1a) is one of the most important Pb–Zn production areas in China. This metallogenic province includes more than 400 Pb–Zn deposits (Liu & Lin 1999; RJ Si, unpub. PhD thesis, Chinese Academy of Sciences, 2005; Wu *et al.* 2013; Zhou *et al.* 2013*c*) and has produced approximately 27% of the total Zn and Pb resources in China over the past decades (e.g. Zhang *et al.* 2015; Zhou *et al.* 2018*a*). Several giant deposits have been found, including the Huize (> 5.0 Mt of Pb+Zn reserves; Zhou *et al.* 2001), Daliangzi (*c.* 3.0 Mt of Pb+Zn reserves; Zheng & Wang, 1991), Maoping (> 2.5 Mt of Pb+Zn reserves; Wei *et al.* 2015), Tianbaoshan (> 2.0 Mt of Pb+Zn reserves; Zhou *et al.* 2013*c*), Nayongzhi (*c.* 1.5 Mt of Pb+Zn reserves; Zhou *et al.* 2018*b*) and Fule (> 1.0 Mt of Pb+Zn reserves; Lü, 2014) Pb–Zn deposits. Among these deposits, the Fule deposit is hosted in the carbonate rocks of the middle Permian Yangxin Formation (Fig. 1b; RJ Si, unpub. PhD thesis, Chinese Academy of Sciences, 2005; Lü, 2014) and spatially and stratigraphically close to the upper Permian Emeishan flood basalts. However, whether the Fule deposit is related to the Emeishan flood basalts has been debated for decades. Some studies have considered that a small portion of the ore-forming materials is derived from Emeishan flood basalts (Liu & Lin 1999; Huang *et al.* 2004). Others researchers have proposed that the Emeishan flood basalts only act as a heat source or barrier layer for the Pb–Zn deposit (Li *et al.* 2012). Due to a lack of understanding of the sources of the ore-forming materials, the genesis type of the Fule deposit remains controversial; previous studies have suggested that it is a sedimentary exhalative (SEDEX) deposit or 'sedimentary reworking-type' deposit (Tu, 1984; Zhao, 1995; Liu & Lin 1999), a Permian Emeishan mantle plume-related Zn–Pb deposit (Xie, 1963; Huang *et al.* 2004), a Mississippi Valley-type (MVT) deposit (e.g. CQ Zhang, unpub. Masters thesis, China University of Geosciences, 2005; ZL Li, unpub. Master thesis, University Chinese Academy of Sciences, 2016; Li *et al.* 2018*a*) or a Sichuan–Yunnan–Guizhou (SYG) -type deposit (Han *et al.* 2007*b*; Zhou *et al.* 2018*c*). Accordingly, the Fule Pb–Zn deposit represents an excellent case study for understanding the origin of ore-forming materials and the mineralization of these Pb–Zn deposits in the SYG area.

Isotope geochemistry is a useful research tool for studying hydrothermal deposits. Sulphur isotopic compositions can be used to determine the origin of S and the isotopic evolution of the

CAMBRIDGE UNIVERSITY PRESS

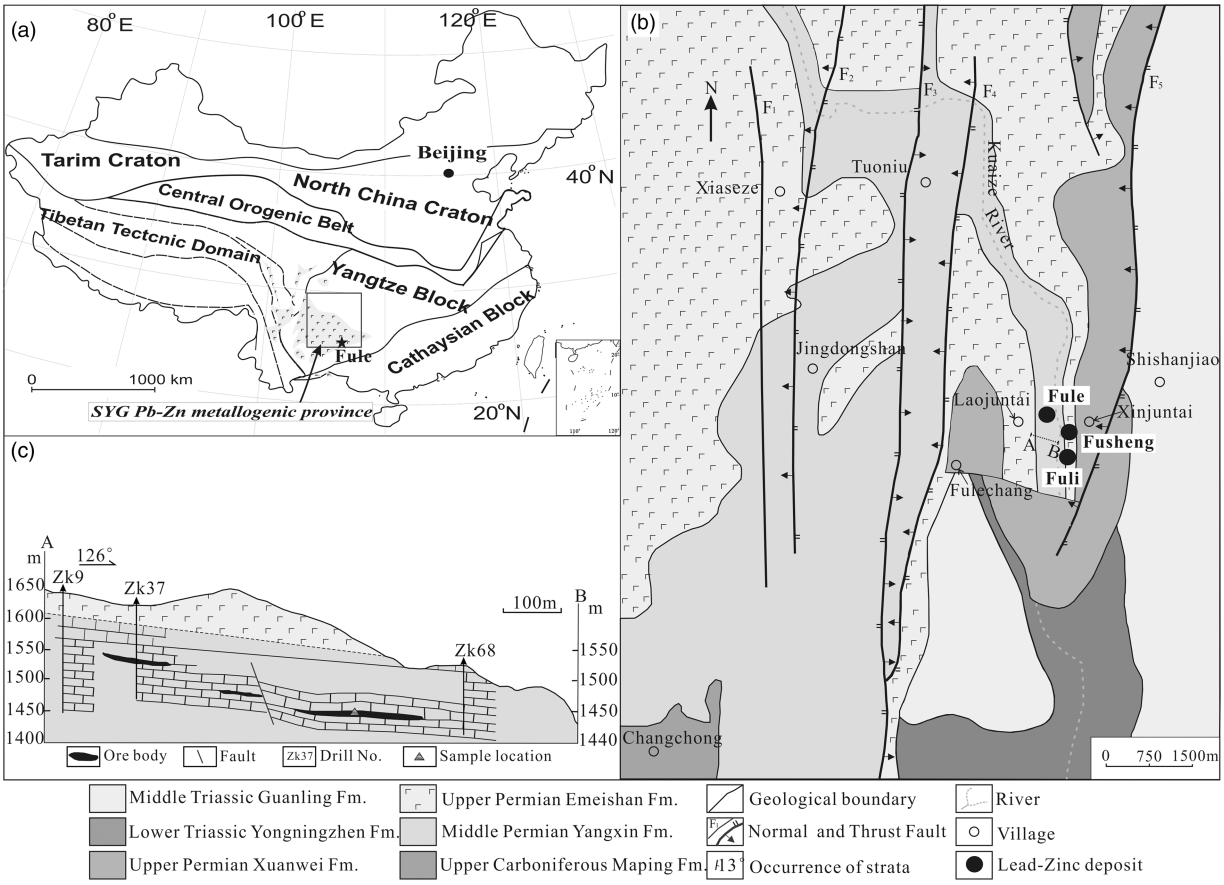

Fig. 1. (**a**) Regional geological location of the Fule deposit and the SYG Pb–Zn metallogenic province (modified after Zhu *et al.* 2017). (**b**) Geological sketch map of the Fule Pb–Zn deposit (modified from Liu & Lin, 1999; Lü, 2014). (**c**) Cross-section of the Fule deposit (modified from RJ Si, unpub. PhD thesis, Chinese Academy of Sciences, 2005).

fluids (Seal, 2006; Barker *et al.* 2009). Sulphur, the 14th most abundant element in the crust, has a stable isotope that can provide insight into the origins of sulphide minerals (Seal, 2006; Haest *et al.* 2010). The sulphur isotopic composition of sulphides is commonly expressed in delta notation (δ), which means $\delta^{34}S = \delta(^{34}S/^{32}S)$ (Seal, 2006). Previous studies of the S isotopes of its sulphides have been based on the traditional bulk powder method (e.g. RJ Si, unpub. PhD thesis, Chinese Academy of Sciences, 2005; Lü, 2014), which probably yields mixed $\delta^{34}S$ values because mineral separation sometimes exceeds the scale of the particle variations in sulphide minerals (e.g. Tang *et al.* 2011, 2014; Ye *et al.* 2016). Such an analytical method may have led to an inaccurate understanding of the S source. Nanoscale secondary-ion mass spectrometry (NanoSIMS) has been widely applied for *in situ* isotope analysis (Zhang *et al.* 2014), which is characterized by high spatiotemporal resolution and analytical sensitivity (Hoppe, 2006; Herrmann *et al.* 2007; Yang *et al.* 2015) and can yield *in situ* S isotopic data ($^{34}S/^{32}S$) from micron- or submicron-scale sulphides (e.g. Gerdes *et al.* 2000; Pósfai *et al.* 2001; Algeo *et al.* 2008; Wacey *et al.* 2011) with high accuracy (Winterholler *et al.* 2006).

In this research, NaonoSIMS was used to analyse the S isotopic compositions of pyrite and sphalerite of the Fule deposit together with geological and mineralogical data to (1) identify the possible source of the reduced sulphur; (2) constrain the mineralizing process in the Fule deposit; and (3) understand the ore genesis of the Fule deposit.

2. Geological setting

2.a. Regional geology

The Fule Pb–Zn deposit in the western Yangtze Block, southwestern China, is located in the southeastern part of the SYG polymetallic metallogenic province (Fig. 1a) and the southern part of the NE Yunnan depression carbonate-bearing basin in the SYG (Han *et al.* 2007*a*). The basin formed during late Sinian time and underwent tectonic uplift during Late Jurassic time (Zhang *et al.* 2005). The regional faults are dominated by NE–SW- and N–S-trending faults, and the basement comprises the Proterozoic Kunyang group, which is mainly formed of metamorphic rocks. The exposed units in this region include Devonian, Carboniferous, Permian and Triassic rocks, all of which are primarily composed of carbonate, basalts and clastic sedimentary rocks. More than 400 Pb–Zn deposits have been found in this area (Liu & Lin, 1999), and these deposits are characterized by high Pb and Zn ore grades, irregular ore bodies, simple mineralogies and weak degrees of alteration (e.g. Zhou *et al.* 2001, 2013*a*). These deposits are mainly hosted in the carbonate strata underlying the upper Permian Emeishan flood basalts (e.g. Huang *et al.* 2004, 2010).

In the Fule mining area, the major structures are NNE–SSW- and N–S-trending faults (Fig. 1b), all of which are reverse faults except F1, which is a normal fault. In particular, the N–S- and NE–SW-trending reverse faults play important roles in controlling the formation, distribution and enrichment of Pb and Zn deposits.

https://doi.org/10.1017/S0016756819000852 Published online by Cambridge University Press

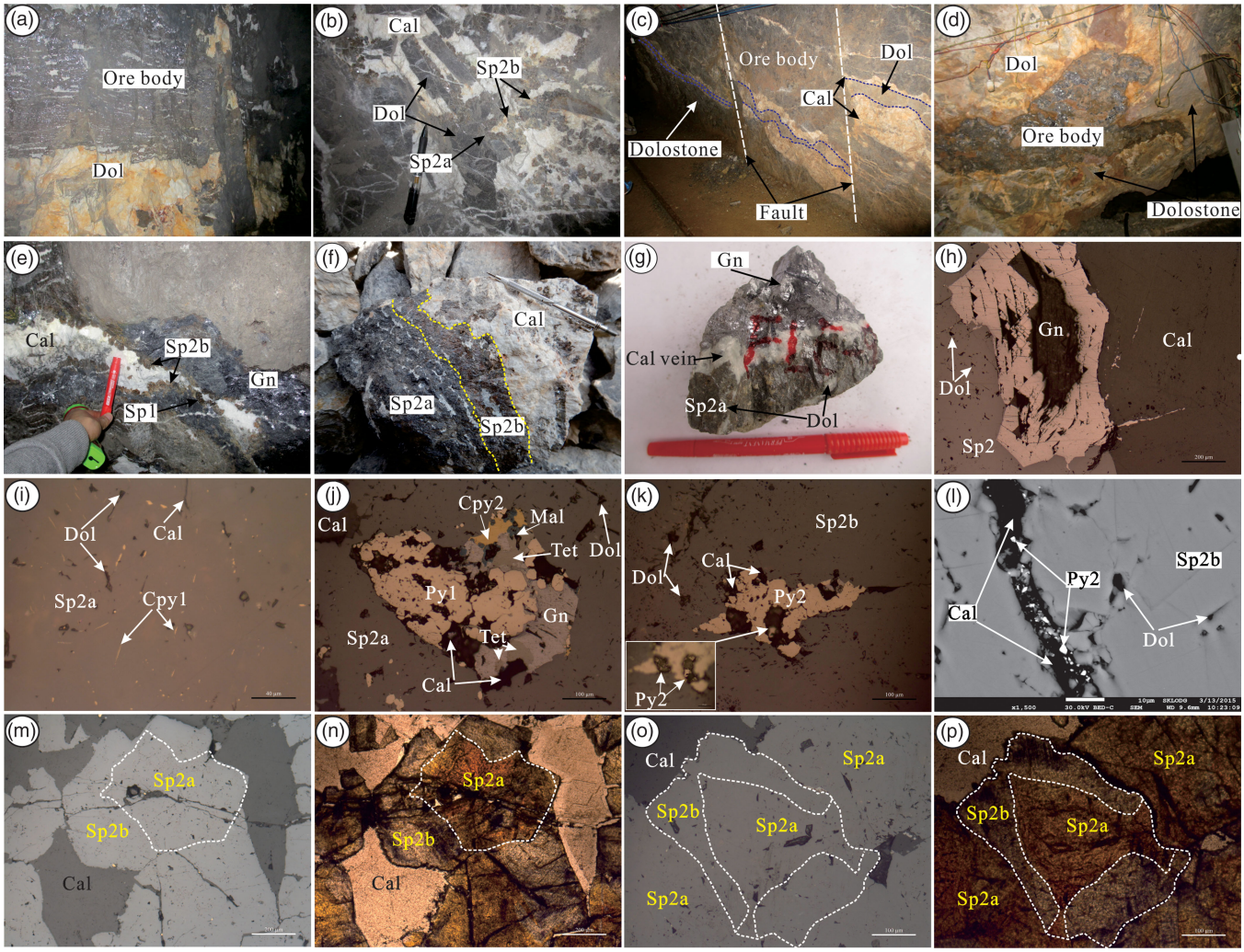

Fig. 2. (Colour online) Field and microscope photographs of ore bodies and mineral paragenesis in the Fule deposit. (**a**) Ore bodies hosted in dolostone and occurring as horizontal stratiform bodies. (**b**) Pb–Zn ores filling in an interlayer fracture. (**c**) Ore bodies strictly controlled by faults and associated with some broken dolomite and calcite veins. (**d**) Pb–Zn ores filling in the open space of a karst cave. (**e**) The principal ore minerals are sphalerite and galena. (**f**) Black-brown sphalerite (Sp2a) formed earlier than brown sphalerite (Sp2b). (**g**) Galena formed later than the other sulphides and replaced by gangue minerals. (**h**) Galena formed later than the sphalerite. (**i**) Emulsion droplet chalcopyrite (Cpy1) distributed in sphalerite as a disease texture, which suggests that they formed during the same stage. (**j**) Anhedral pyrite (Py1) was replaced by late sulphide minerals (including galena, chalcopyrite (Cpy2), tetrahedrite and malachite). (**k**) Euhedral pyrites (Py2) intergrown with calcite in fissures of sphalerite. (**l**) Aggregates of pyrites (Py2) filling in a calcite vein (backscattered image). (**m**) Single sphalerite particle under reflected light. (**n**) Sphalerite has different colours from core to rim (transmitted light), corresponding to black-brown (Sp2a), brown (Sp2b) and light yellow (Sp2c) sphalerite, respectively. (**o**) Sphalerite under reflected light. (**p**) Sphalerite has two mineralization stages under transmitted light. Sp – sphalerite; Gn – galena; Py – pyrite; Cpy – chalcopyrite; Tet – tetrahedrite; Ma – malachite; Cal – calcite; and Dol – dolomite.

2.b. Geology of the Fule deposit

Ordovician, Silurian, Upper Triassic and some Tertiary strata are absent from the Fule mining district. The stratigraphic sequence consists of the upper Carboniferous Maping Formation, middle Permian Yangxin Formation, upper Permian Emeishan Formation, upper Permian Xuanwei Formation, Lower Triassic Yongningzhen Formation, Middle Triassic Guanling Formation and some Quaternary rocks (Fig. 1b). The upper Carboniferous Maping Formation is composed of light grey and thick-bedded limestone with some coarsely crystalline dolostone. The middle Permian Yangxin Formation is the main ore-hosting unit, and its thickness exceeds 1 km. This formation is dominated by alternating grey (light to dark) dolostone and limestone and contains some flint nodules in the uppermost layer. The upper Permian Emeishan Formation, which is > 2 km thick and predominantly consists of vesicular, amygdaloid basalts and volcanic breccia, unconformably overlies the middle Permian Yangxin Formation. The upper Permian Xuanwei Formation consists of mudstone and sandstone. The Lower Triassic Yongningzhen Formation conformably overlies the upper Permian clastic rocks and is chiefly composed of light grey limestone and clastic rocks. The Middle Triassic Guanling Formation consists primarily of sandstone, mudstone and dolostone. The wall rock of the ore bodies is dominated by dolostone and minor limestone (Fig. 1b, c).

A total of 20 ore bodies have been recognized in the Fule deposit, and their elevations range from 1450 to 1536 m (Fig. 1c). These ore bodies have a general trend of NW–SE, and the mining area is approximately 3 km long and 1.5 km wide. These ore bodies commonly occur as stratiform, lenticular (Fig. 1c) and veined bodies along the bedding planes of the middle Permian Yangxin Formation (Figs 1c, 2a), and are occasionally hosted in fracture zones (Fig. 2b). These ore bodies are strictly

https://doi.org/10.1017/S0016756819000852 Published online by Cambridge University Press

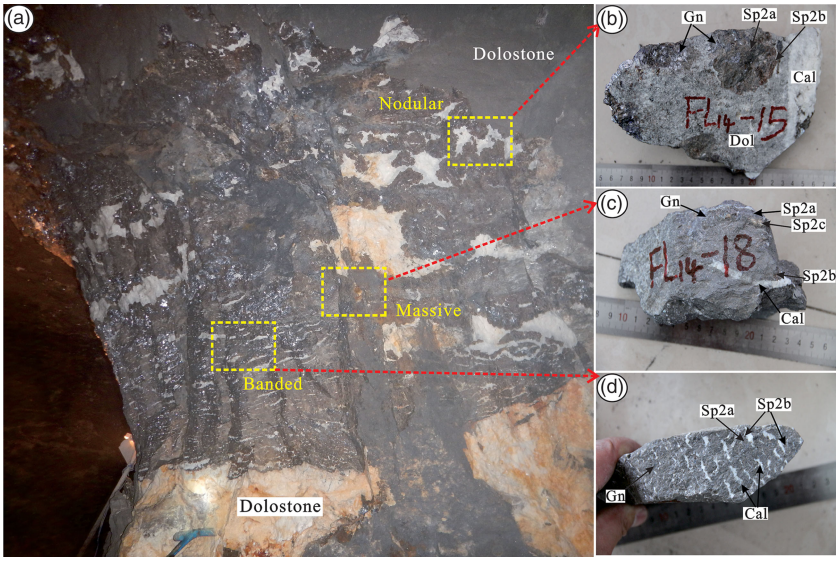

Fig. 3. (Colour online) Sampling locations of the ores. (**a**) The overall view of the ore body. (**b–d**) Samples with different ore structures, that is, (b) nodular, (c) massive and (d) banded structures.

MINERAL	Diagenetic stage	Hydrothermal stage Sulphide + carbonate				Supergene stage
Mineral assemblage	Dol+Cal	Sp+Gn+Py (Cpy+Tet+Tt)+Dol+Cal				Oxidized minerals
Generation		I	II		III	
Pyrite replaced by later sulphides (Py1)						
Black-brown sphalerite (Sp2a)						
Brown sphalerite (Sp2b)						
Light-yellow sphalerite (Sp2c)						
Emulsion droplet chalcopyrite(Cpy1)						
Pyrite in calcite vein (Py2)						
Galena						
Chalcopyrite(Cpy2)						
Zn-tennantite						
Tetrahedrite						
Dolomite						
Calcite						
Malachite						
Smithsonite						

Less More

Fig. 4. Paragenetic sequence of the minerals in the Fule deposit.

controlled by faults (Fig. 2c) and many breccias can be found around karstic caves, which were affected by faults. Some Pb–Zn ores cemented the breccias or filled in the open space within karst caves (Fig. 2d).

2.c. Mineralogy and paragenesis

The principal ore minerals are sphalerite and galena (Fig. 2e–g), with minor pyrite (under microscopy and scanning electron microscopy, Fig. 2j–l) and Cu-bearing minerals (Fig. 2i, j). Some oxidized ores, including smithsonite and malachite, are also present (Fig. 2j). The gangue minerals are composed of dolomite and calcite (Fig. 2c). The sulphides are fine to coarse grained, with anhedral to euhedral granular textures. The ore structures are dominated by nodular (Fig. 3b), massive (Fig. 3c), banded (Fig. 3d), disseminated and veined structures. Dolomitization and calcitization are present in the wall rock.

The mineralization process can be divided into three stages (Fig. 4): (1) diagenetic stage, dolomite + calcite; (2) hydrothermal stage, sulphides + dolomite + calcite; and (3) supergene stage, oxidized minerals. The sulphides of the deposit are mainly formed in the hydrothermal stage, which can be further divided into three generations: (1) generation 1, fine pyrite + dolomite + calcite; (2) generation 2, sphalerite + galena + coarse pyrite + emulsion droplet chalcopyrite + dolomite + calcite; and (3) generation 3, chalcopyrite + tetrahedrite + Zn-tennantite + dolomite + calcite.

https://doi.org/10.1017/S0016756819000852 Published online by Cambridge University Press

The microscopic observations reveal several key findings. (1) There are two types of Cu-bearing minerals in the Fule deposit. The first type is the early-formed emulsion droplet chalcopyrite (distributed in sphalerite with an exsolution texture that simultaneously formed in generation 2 with sphalerite, labelled Cpy1 in Fig. 2i). The second type of Cu-bearing minerals is relatively late-formed (generation 3) and replaced the early sulphides (sphalerite, galena and pyrite), including chalcopyrite (Cpy2), tetrahedrite (Tet), Zn-tennantite (Tt) and malachite (Mal) (Li *et al.* 2018*b*). (2) The pyrites are divided into two types, both of which formed in hydrothermal stage. The first type of pyrite (Py1) formed in generation 1, was replaced by later sulphides (sphalerite, galena and Cu-bearing minerals, Fig. 2j) and appears as anhedral granules. The second type of pyrite (Py2, formed in the latter stages of generation 2) mainly replaced sphalerite (Fig. 2k) and is present as fine veins in calcite (Fig. 2l). This type of pyrite formed later than the other sulphide minerals and occurs as subhedral–euhedral granules, such as cubic (close-up image in Fig. 2k) and pyritohedron granules (Fig. 2l). (3) In addition, three types of sphalerite (Fig. 2e) were observed under the microscope under transmitted light (Fig. 2n, p and Fig. 5d–f) and formed in generation 2. From early to late (i.e. core to rim), the generation sequence is black-brown sphalerite (Sp2a), brown sphalerite (Sp2b) and light yellow sphalerite (Sp2c) (Fig. 2f, m–p).

Based on the macro- to micro-scale geological observations related to the generation sequence, replacement and colours of minerals, the mineralization stages in the Fule deposit were divided into diagenetic, hydrothermal (sulphide + carbonate) and supergene stages, and the simplified paragenetic sequence (Fig. 4) of the sulphide minerals is:

Pyrite (Py1) → sphalerite (Sp2a → Sp2b → Sp2c) + emulsion droplet chalcopyrite (Cpy1) → pyrite (Py2) → galena (Gn) → Cu-bearing minerals (Cpy2, Tet, Tt, Mal).

3. Samples and analytical methods

The sampling locations are shown in Figure 3a. Three sulphide samples representative of nodular (Fig. 3b), massive (Fig. 3c) and banded (Fig. 3d) ores were chosen. Diverse types of pyrite (Py1 and Py2) and sphalerite (Sp2a, Sp2b and Sp2c) were selected for *in situ* S isotopic analysis. Because no galena standard was available (e.g. Zhang *et al.* 2014), the *in situ* S isotopic compositions of galena were not obtained in this study. The polished thin-sections were observed with a transflective optical microscope in the Institute of Geochemistry, Chinese Academy of Sciences, Guiyang, China. *In situ* S isotopic analyses were performed at the NanoSIMS Laboratory of the Institute of Geology and Geophysics, Chinese Academy of Science, Beijing, using a Cameca NanoSIMS 50L.

This experiment used an FC-EM-EM-EM model (Yang *et al.* 2015) to meet the spatial resolution requirements. ^{32}S was counted with a Faraday cup (FC), while ^{33}S, ^{34}S and ^{36}S were counted with an electronic multiplier (EM) (Zhang *et al.* 2014). High-resolution images of the distributions of seven elements and isotopes (^{32}S, ^{34}S, ^{63}Cu, ^{75}As, ^{80}Se, ^{197}Au and ^{208}Pb) were simultaneously obtained. During the measurement process, (1) the thin-sections were carbon-coated for conductivity at high voltage and placed in the sample compartment; (2) a Cs^+ primary ion beam with 7 pA (impact energy of 16 keV) and a diameter of 0.3 μm rastered across the sample surface, sputtering out positive and negative secondary ions that were separated in the magnetic field based on their mass-to-charge ratios; (3) the signals (seven elements or isotopes) were detected by seven FCs or EMs; and (4) a 20 × 20 μm analysis area was eroded with two or three spots (1.5 × 1.5 μm) being chosen for analysis in the eroded area (Fig. 6). For more details about these operating conditions, refer to Zhang *et al.* (2014) and Yang *et al.* (2015).

The standards used in this study were pyrite grains collected from a drill core (ZK117) from Qulong, Tibet, China, and sphalerite grains collected from Mengya's skarn Pb–Zn deposit, eastern Gangdese metallogenic belt, China. All of these standards have been calibrated by international standards included Balmat (pyrite and sphalerite) and CAR 123 (pyrite) (Zhang *et al.* 2014). The pyrite and sphalerite standards are PY-1117 ($\delta^{34}S_{VCDT}$ = 0.3, SD (1σ) = 0.01) and MY09-12 ($\delta^{34}S_{VCDT}$ = 3.1, SD (1σ) = 0.06), respectively. The analytical precision calculated from replicate analyses was better than 0.2‰ (1σ). The S isotopic analyses comprised 102 analyses on pyrite and 61 analyses on sphalerite from different stages of the mineralization process. The results are summarized in Table 1 and online Supplementary Table S1 (available at http://journals.cambridge.org/geo) and shown in Figs 5–8.

4. Analytical results

4.a. S isotopic compositions

Sulphide minerals were analysed to assess their generation sequence, and a total of 163 analyses (102 pyrite and 61 sphalerite analyses) were obtained (Table 1, online Supplementary Table S1 and Figs 7, 8). The overall $\delta^{34}S$ values of pyrite and sphalerite in the Fule deposit range from +16.1 to +23.0‰, which represents a wider range than the values obtained from bulk analysis of sphalerite and galena (+10.04 to +16.43‰; Zhou *et al.* 2018*a*). In this study, we correlate the *in situ* S isotopic data with the generation sequence of sulphide minerals (Figs 2, 5). The S isotopic values of sulphides are not obviously correlated with their generations (Fig. 8), that is, the early-stage pyrite (Py1) (+18.4 to +20.7‰; average, +19.3‰; n = 18) was replaced by sphalerite (specifically, black-brown sphalerite (Sp2a) (+17.1 to +19.2‰; average, +18.1‰; n=5) → brown sphalerite (Sp2b) (+18.1 to +22.1‰; average, +19.8‰; n=24) → light yellow sphalerite (Sp2c) (+18.2 to +22.4‰; average, +20.1‰; n=32)), which was in turn replaced by late-stage pyrite (Py2) (+16.1 to +23.0‰; average, +20.3‰; n = 84), which is present as fine veins. The $\delta^{34}S$ values of different stages exhibit partial overlap (Fig. 7a) but show a smaller difference. The main $\delta^{34}S$ concentrations (Fig. 8) range from +17.3‰ to +18.8‰ with an average of +18.1‰ (Sp2a) → +18.6‰ to +20.8‰ with an average of +19.8‰ (Sp2b) → +18.9‰ to +21.0‰ with an average of +20.1‰ (Sp2c) → +19.2‰ to +22.3‰ with an average of +20.3‰ (Py2) (Fig. 8). The $\delta^{34}S$ values of single crystals of sphalerite (Fig. 5f) and pyrite (Fig. 5c) from cores to rims show a weak increased trend, that is, +19.1 to +19.4‰ (average, +19.3‰) → +20.7 to +20.8‰ (average, +20.8‰) for sphalerite and +19.0 to +19.5‰ (average, +19.3‰) → +20.0 to +20.6‰ (average, +20.2‰) for pyrite.

4.b. Distribution characteristics of elements in pyrite and sphalerite

The element distribution images of ^{32}S, ^{34}S, ^{63}Cu, ^{75}As, ^{80}Se, ^{197}Au and ^{208}Pb are shown in Figure 6. These elements are uniformly

https://doi.org/10.1017/S0016756819000852 Published online by Cambridge University Press

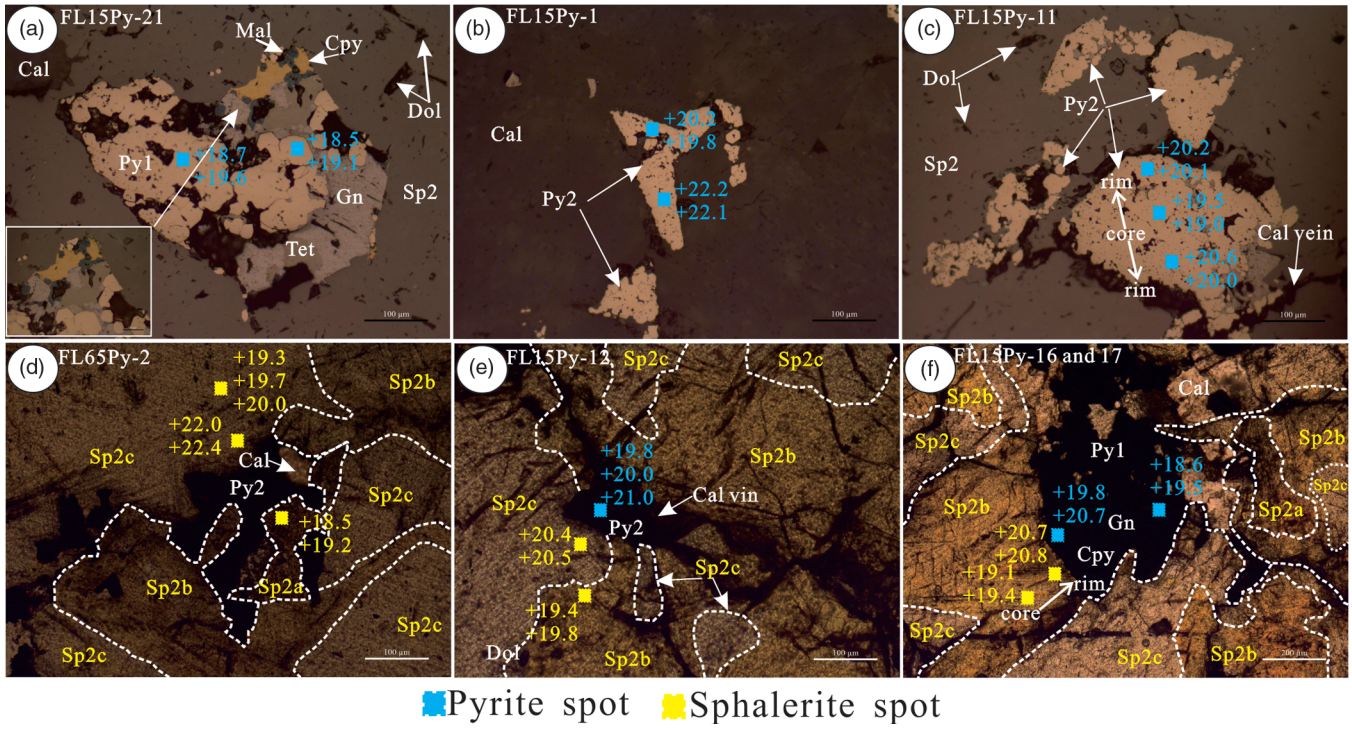

Fig. 5. (Colour online) The analysed locations and $\delta^{34}S$ values of pyrite and sphalerite in the Fule deposit. (**a**) Anhedral pyrite (Py1) was replaced by later sulphides and showed relative lower $\delta^{34}S$ values than the subhedral–euhedral pyrites (Py2) shown in (**b**). (**c**) The $\delta^{34}S$ values of subhedral pyrite (Py2) exhibit a weakly increasing trend from core to rim. The $\delta^{34}S$ values of sphalerite under transmitted light: (**d**) no difference between black-brown (Sp2a), brown (Sp2b) and light-yellow (Sp2c); (**e**) no difference between the $\delta^{34}S$ values of sphalerite and pyrite; and (**f**) the $\delta^{34}S$ values of sphalerite are weakly increased from the early to late mineralization stages.

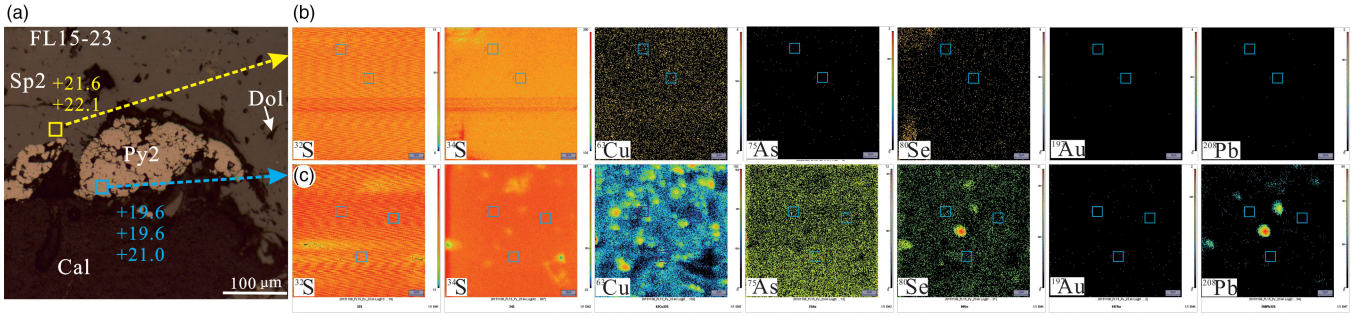

Fig. 6. (Colour online) The mapping of characteristic elements in the pyrite and sphalerite in the Fule deposit: (**a**) analysed locations of the sulphides (under microscope); and (**b**, **c**) element maps of sphalerite and pyrite, respectively.

distributed in the sphalerite (Fig. 6b), implying that ^{63}Cu, ^{75}As, ^{80}Se and ^{208}Pb exhibit isomorphism in the sphalerite.

The isotopes of ^{32}S, ^{34}S and ^{75}As show homogeneous isotopic compositions in pyrite (Fig. 6c), whereas ^{63}Cu, ^{208}Pb and ^{80}Se are unevenly distributed in pyrite; this likely indicates that these elements exist as micro- or nano-inclusions in the pyrite.

5. Discussion

5.a. Sulphur origin

Sulphur isotopic compositions provide strict constraints on the origin of reduced S in hydrothermal fluids and the genetic processes of mineralization (Ohmoto & Rye 1979; Carr *et al.* 1995; Haest *et al.* 2010). The striking S isotopic signatures of the pyrite and sphalerite in the Fule deposit are both enriched in heavy S isotopes, and their values largely overlap (Table 1, online Supplementary Table S1 and Figs 7, 8), implying that the pyrite and sphalerite may stem from the same source.

Previous researchers have proposed that many non-traditional stable isotopes, such as Fe, Zn and Cd, increase gradually with metal precipitation. The early precipitates are therefore enriched in light isotopes and the late ones are enriched in heavy isotopes, which could be interpreted as reflecting kinetic Rayleigh fractionation (e.g. Beard *et al.* 2003; Ellis *et al.* 2004; Kelley *et al.* 2009). The main $\delta^{34}S$ values from early to late stage (Fig. 8) and from the cores to rims in some single sulphide crystals show a slight increasing trend (Figs 5c, f), implying that partial Rayleigh fractionation (e.g. Tang *et al.* 2014; Zhu *et al.* 2017) took place in the Fule deposit. In this scenario, the early precipitation of sulphides (core) has relatively enriched ^{32}S, and the remaining fluid has relatively higher ^{34}S values (rim), which could be interpreted as an open system.

https://doi.org/10.1017/S0016756819000852 Published online by Cambridge University Press

Table 1. Analysed results of the $\delta^{34}S$ values of sphalerite and pyrite in the Fule deposit. SD – standard deviation.

Hydrothermal generation	Mineral	Characteristics	$\delta^{34}S_{cor}$ (‰)			
			Min	Max	Mean	SD
I	Pyrite (Py1)	Anhedral granule, replaced by sphalerite, galena and Cu-bearing minerals	18.4	20.7	19.3	0.6
II	Sphalerite (Sp2a)	Black-brown	17.1	19.2	18.1	0.9
	Sphalerite (Sp2b)	Brown	18.1	22.1	19.8	1.3
	Sphalerite (Sp2c)	Light yellow	18.2	22.4	20.1	1.3
III	Pyrite (Py2)	Subhedral–euhedral granule, replaces sphalerite	16.1	23.0	20.3	1.6

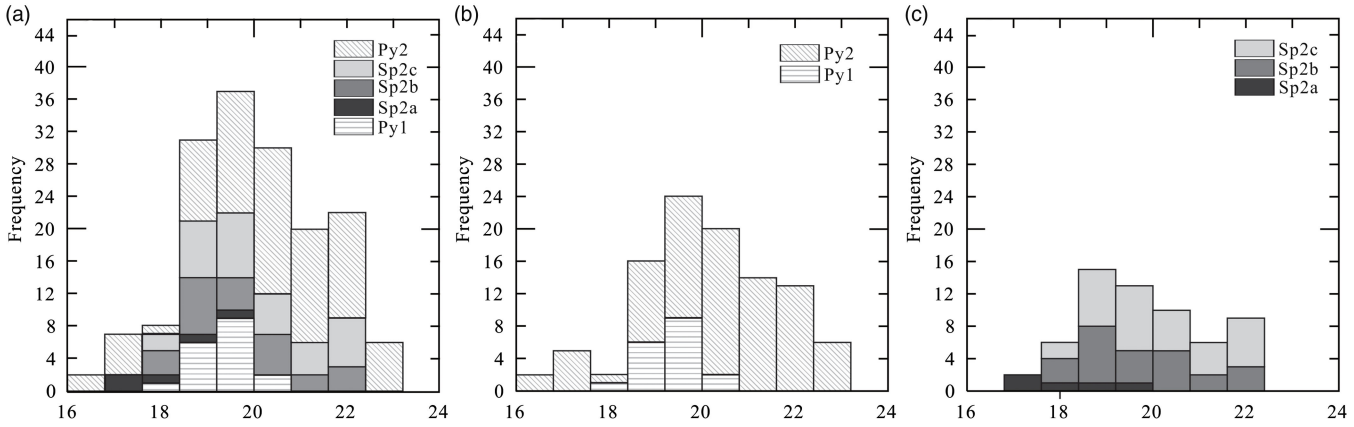

Fig. 7. Histograms of S isotopic compositions in the Fule deposit: (**a**) sulphide minerals in different stages; (**b**) of pyrite; and (**c**) of sphalerite.

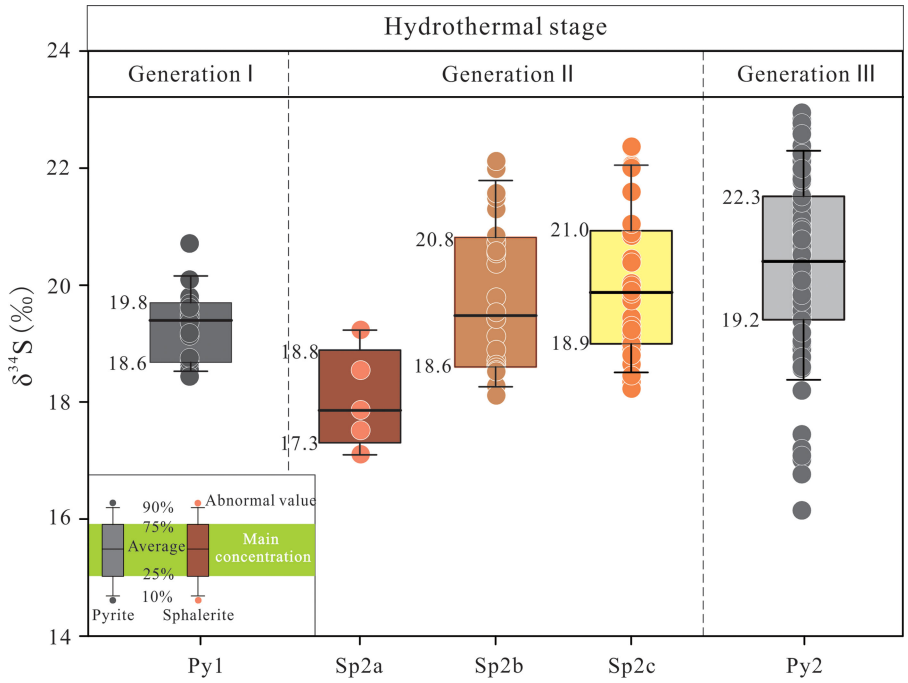

Fig. 8. (Colour online) Box plot of the $\delta^{34}S$ values of sulphide minerals based on generation sequence.

https://doi.org/10.1017/S0016756819000852 Published online by Cambridge University Press

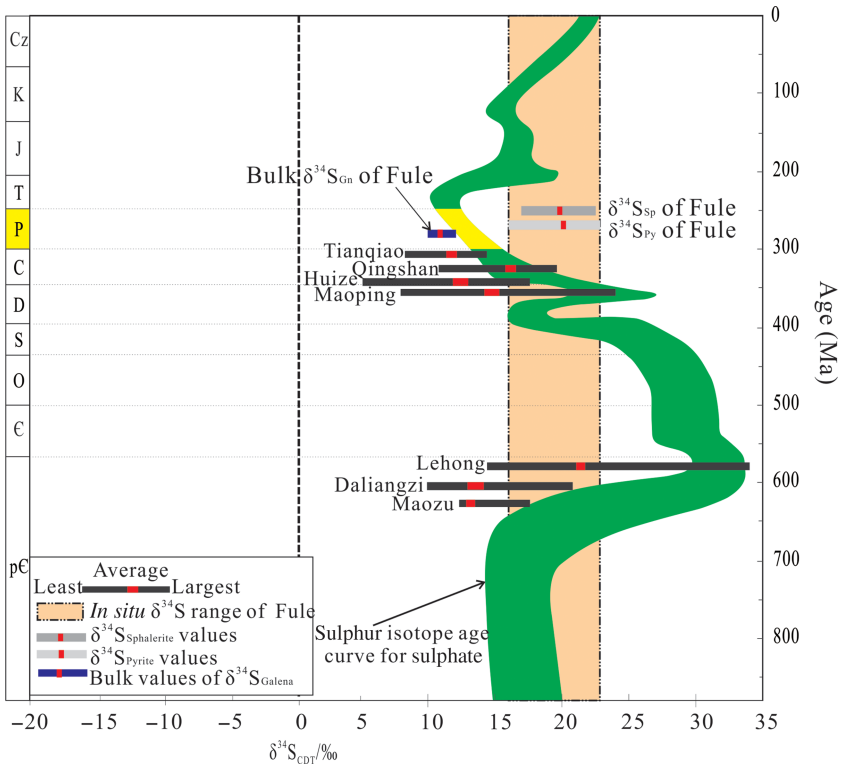

Fig. 9. (Colour online) The S isotopic compositions of Pb–Zn deposits in the main ore-bearing strata of the Sichuan–Yunnan–Guizhou (SYG) metallogenic province, modified after Claypool *et al.* (1980).

The S isotopic compositions of the sulphides could have been affected by the temperature, pH and fO_2 of the fluids as well as by the S isotopic composition of the fluids (Sakai, 1968; Ohmoto, 1972). Even if the pH and fO_2 did not significantly change, the $\delta^{34}S$ values of the pyrite also have a large range (Ohmoto, 1972) in their stability field; the narrow range of $\delta^{34}S_{pyrite}$ values in the Fule deposit should therefore not have been constrained by pH and fO_2. Interestingly, previous studies have considered that the degree of S isotopic fractionation between different S species (e.g. H_2S, ZnS, PbS and FeS_2) is less than 3‰ when ore-forming temperatures are lower than 350 °C (Ohmoto, 1972; Peevler *et al.* 2003). Hence, the narrow range of $\delta^{34}S$ values in the sulphides (Table 1, online Supplementary Table S1 and Figs 7, 8) of the Fule deposit was more likely to have been controlled by the ore-forming temperature than pH or fO_2. Furthermore, the S isotopic compositions of the sulphides were also affected by those of the ore-forming fluids.

The *in situ* S isotopic compositions of galena were not obtained in this study, due to the lack of a galena standard. Furthermore, the $\delta^{34}S$ values of the galena from bulk traditional analysis (+10.04 to +11.86‰, Zhou *et al.* 2018*a*) that were significantly lower than the $\delta^{34}S$ values of pyrite and sphalerite (+16.1 to +23.0‰) in the Fule deposit. The sulphides (sphalerite, galena and pyrite) often enclose a lot of micro-gangue minerals (e.g. dolomite) and sulphide minerals (e.g. sphalerite and pyrite; Fig. 2h–l), suggesting that the bulk S isotope analysis represents a mixed value. The *in situ* $\delta^{34}S$ values of the pyrite and sphalerite (+16.1 to +23.0‰) could therefore represent the real $\delta^{34}S$ values of the Fule deposit. The potential sources of S in hydrothermal mineralization contain mantle-derived S (0‰, Chaussidon *et al.* 1989) and marine sulphate (*c.* 20‰). The $\delta^{34}S$ values of the Fule deposit range from +16.1 to +23.0‰, which are similar to the value of marine sulphate (gypsum and barite, +12.9‰ to +25.9‰; Ren *et al.* 2018), indicating that the S in the Fule deposit derived from marine sulphate. Primary sulphides in the Fule deposit are composed of sphalerite, galena, pyrite with minor Cu-bearing minerals; however, sulphate is lacking in the Fule paragenetic assemblage. Generally, because sulphates were not observed in the paragenetic assemblage, the $\delta^{34}S$ values of sulphides could be equivalent to that of the responsible ore fluids. The $\delta^{34}S$ values of the sulphides therefore represent the total $\delta^{34}S$ values of the ore-forming fluids (Ohmoto, 1972; Pinckey & Rafter 1972; Seal, 2006), that is, $\Sigma\delta^{34}S_{fluid}$ *c.* $\Sigma\delta^{34}S_{sulphides}$ *c.* +16.1 to +23.0‰.

Numerous studies (e.g. CQ Zhang, unpub. Master thesis, China University of Geosciences, 2005; Zhou *et al.* 2010, 2012, 2013*b*; Shentu *et al.* 2011; Zhong *et al.* 2013; Yuan *et al.* 2014) have shown that the S isotopes of the Pb–Zn deposits in different strata in the SYG province are basically consistent with those of coeval marine sulphates (Fig. 9, Table 2). Namely, the S in these Pb–Zn deposits principally originated from the S in the ore-bearing strata (e.g. Liu, 1995; CQ Zhang, unpub. Master thesis, China University of Geosciences, 2005; CQ Zhang, unpub. PhD thesis, Chinese Academy of Geological Sciences, 2008; Zhou *et al.* 2013*a*). The *in situ* S isotopic analyses of the Fule deposit have shown that the $\delta^{34}S$ values of the sulphide minerals vary from +16.1‰ to +23.0‰, which are higher than the $\delta^{34}S$ value of the marine sulphate in the Permian rocks (*c.* +11‰, Claypool *et al.* 1980) but largely similar to that of the sulphates (gypsum and barite) over a broader area older than the Permian strata (+12.9‰ to +25.9‰, Ren *et al.* 2018). Even if sulphur originated entirely from Permian marine sulphate (*c.* +11‰), the theoretical $\delta^{34}S$ values of these sulphides could drop to −4‰ based on the effect of TSR for S isotopic fractionation (0‰ to 15‰; Ohmoto, 1972). The theoretically predicted $\delta^{34}S$ values of these sulphides range from −4‰ to +11%, which does not correspond well with the $\delta^{34}S$ values observed in our study. The $\delta^{34}S$ values of the sulphates (gypsum and barite) hosted in the regional rocks are +12.9‰ to +25.9‰ and match the observed results reasonably

https://doi.org/10.1017/S0016756819000852 Published online by Cambridge University Press

Table 2. S isotopic compositions of Pb–Zn deposits in the main ore-bearing strata of the SYG province. Py – Pyrite; Sp – Sphalerite; and Gn – Galena.

Deposit	Host strata	Wall rock	Analysis mineral	Data number	Min	Max	Mean	References
Fule	Permian	Dolostone	Sp	61	17.1	22.4	19.8	This paper
			Py	102	16.1	23.0	20.1	
			Gn	4	10.04	11.86	10.76	Zhou *et al.* 2018*a*
Tianqiao	Carboniferous	Dolostone	Py Sp Gn	35	8.35	14.44	11.71	Zhou *et al.* 2010
Qingshan	Carboniferous	Dolostone	Py Sp Gn	27	10.7	19.6	16.09	Zhou *et al.* 2013*b*
Huize	Devonian–Carboniferous	Dolostone	Sp Gn	134	4.8	17.4	12.2	Zhong *et al.* 2013
Maoping	Devonian–Carboniferous	Dolostone	Py Sp Gn	19	7.96	24.1	14.72	Shentu *et al.* 2011
Lehong	Late Ediacaran	Dolostone	Sp Gn	4	14.1	34	21.3	Zhang (unpub. Master Thesis, China University of Geosciences, 2005)
Daliangzi	Late Ediacaran	Dolostone	Sp Gn	12	9.7	20.6	13.53	Yuan *et al.* 2014
Maozu	Late Ediacaran	Dolostone	Py Sp Gn	12	13.3	15.4	13.4	Zhou *et al.* 2012

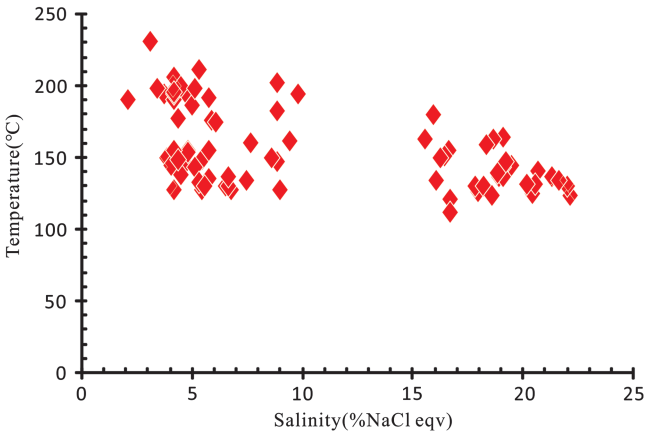

Fig. 10. (Colour online) The scatter diagrams of the (**a**) homogenization temperatures and (**b**) salinities of fluid inclusions in the sphalerite of the Fule deposit (data from ZL Li, unpub. Master thesis, University of Chinese Academy of Sciences, 2016).

well (+16.1‰ to +23.0‰), which can be attributed to low fractionation of $\Delta\delta^{34}S_{\text{sulphate-sulphide}}$. The S of the Fule deposit may therefore have been chiefly derived from the marine sulphates in regional rocks. The ore-forming fluid flowed through the regional strata and mixed with sulphates with different S compositions. The S source of the Fule deposit is significantly different from that of most other Pb–Zn deposits, which originated primarily from the ore-bearing strata in the SYG Pb–Zn mineralization province.

Seal (2006) found $\delta^{34}S$ values of approximately 20‰ for sulphides in MVT deposits, which coincides with those of the composition of the associated sulphates and produced by TSR (Kesler, 1996). The $\delta^{34}S$ values of pyrite and sphalerite in the Fule deposit range from +16.1 to +23.0‰, which coincide with the sulphates hosted in the regional area rocks (+12.9 to +25.9‰, Ren *et al.* 2018). Moreover, some organic materials (e.g. bitumen and CH_4) were found in the Fule deposit (RJ Si, unpub. PhD thesis, Chinese Academy of Sciences, 2005; Lü, 2014), which could participate in TSR and fractionate 0–10‰ (Orr, 1974; Kiyosu, 1980). The sulphate reduction likely caused kinetic Rayleigh fractionation. Combined with previous studies (Barton, 1967; Merce *et al.* 2004), the appropriate chemical reactions are as follows:

$$SO_4^{2-} + CH_4 = H_2S + CO_3^{2-} + H_2O \quad (1)$$

$$M^{2+} + H_2S = 2H^+ + MS\downarrow \quad (2)$$

where M represents metallic elements such as Zn, Pb and Cu.

5.b. Mineralization process of the Fule deposit

The S in sulphate mainly enters the fluid in the form of reduced S, and the possible precipitation mechanisms of reduced S are bacterial sulphate reduction (BSR) and thermochemical sulphate reduction (TSR) (Seal, 2006). BSR occurs at relatively low temperatures (with an optimum temperature of 30–40 °C; Seal, 2006), but the mineralization temperatures (111–232 °C; ZL Li, unpub. Master thesis, University Chinese Academy of Sciences, 2016) of the Fule deposit are higher than the bacterial survival temperature; BSR therefore played a minor role in the mineralization process of the Fule deposit. Generally, BSR results in a product enriched in light isotopes (Seal, 2006; Xue *et al.*, 2015); the sulphides that are produced by BSR therefore have negative S isotopic values. BSR can produce sulphate-sulphide fractionations that typically range from 15‰ to 46‰ (Canfield & Teske 1996; Habicht *et al.* 1998). In contrast, the $\delta^{34}S$ values of the Fule deposit are significantly positive and exist within a narrow range, implying that BSR likely played no role in the mineralization process of the Fule deposit. In contrast, TSR normally occurs at relatively high temperatures (100–140 °C; Machel *et al.* 1995; Worden *et al.* 1995), and its S isotopic fractionation is 0–20‰ (Kiyosu & Krouse 1990; Machel *et al.* 1995). Abundant reduced S can be produced by TSR, and the $\delta^{34}S$ values produced by TSR are relatively stable (Ohmoto *et al.* 1990). TSR is likely the main mechanism of the Fule deposit, and this conclusion is supported by the following aspects: (1) the homogenization temperatures of sphalerite inclusions from the Fule deposit range from 111 to 232 °C (average, 157 °C; Fig. 10; data from ZL Li, unpub. Master thesis, University

https://doi.org/10.1017/S0016756819000852 Published online by Cambridge University Press

Chinese Academy of Sciences, 2016); (2) TSR can produce a large amount of reduced S, consistent with the Pb–Zn reserves of the Fule deposit (> 1 Mt), which require abundant reduced S; and (3) the $\delta^{34}S$ values of the sulphates (gypsum and barite) hosted in the regional rocks (+12.9‰ to +25.9‰) match the observed values well (+16.1‰ to +23.0‰), suggesting that the $\delta^{34}S$ values of the deposit were influenced by the small degree of fractionation produced during the TSR reaction (normally 0–20‰).

The Fule deposit is a typical deposit hosted in Permian strata in the SYG province (CQ Zhang, unpub. Master thesis, China University of Geosciences, 2005; Lü, 2014; ZL Li, unpub. Master thesis, University Chinese Academy of Sciences, 2016; Li *et al.* 2018*a*). The fluid inclusion analyses (Fig. 10; data from ZL Li, unpub. Master thesis, University Chinese Academy of Sciences, 2016) showed that there were at least two types of ore-forming fluids, and this is in accordance with the evidence from *in situ* Pb isotope that the metal Pb was derived from a well-mixed source (basalts, sedimentary and metamorphic rocks; Zhou *et al.* 2018*a*), implying that fluid mixing was the main mechanism responsible for Pb–Zn precipitation in the deposit. With the precipitation of sulphides, acid is produced by fluid mixing (Anderson, 1983); this process explains the widespread occurrence of carbonatization and dissolution-related collapse breccias in the Fule deposit. The base metal sources of the Pb–Zn deposits in the SYG province originated primarily from the folded basement (e.g. Huang *et al.* 2004; Han *et al.* 2007*b*; Zhou *et al.* 2013*a*). The hydrothermal mineralization process of the Fule deposit can therefore be described as follows: the marine sulphates hosted in the regional rocks produced reduced S by the TSR reaction. When the metalliferous fluids (carrying abundant Pb and Zn) migrated upwards along the tectonic channel, they then mixed with a H_2S-rich fluid from the regional strata, resulting in the precipitation of metallic sulphides in the middle Permian Yangxin Formation where the faults and carbonate rocks are well developed.

5.c. Ore genesis

The sulphur source is important for MVT deposits because sulphur is critical for the deposition of metals, and the reduced sulphur is important for the precipitation of sulphide minerals in MVT deposits. Consequently, the sulphur source could indicate the genesis and mineralization of the deposit. Most of the MVT deposit metals were extracted from the basement, and the reduced sulphur was derived from the reduction of marine sulphate by TSR; fluid mixing is the main mechanism of precipitation for metallogenic materials, such as lead and zinc in MVT deposits (Leach *et al.* 2006; Leach & Taylor, 2009).

Numerous studies have shown that most of the Pb–Zn deposits in the SYG area are MVT deposits, including Huize (Han *et al.* 2007*a*), Tianbaoshan (Ye *et al.* 2016), Daliangzi (Yuan *et al.* 2014), Maoping (Wei *et al.* 2015), Wusihe (Xiong *et al.* 2018) and Jinshachang (Bai *et al.* 2013) deposits. Interestingly, the Fule deposit is hosted in the middle Permian Yangxin Formation, and the distance between the Fule Pb–Zn ore bodies and upper Permian Emeishan flood basalts is less than 50 m (Fig. 1c). Some authors have suggested that the upper Permian Emeishan flood basalts played an important role in the formation of the Fule deposit (Si *et al.* 2006; Zhou *et al.* 2018*a*); however, typical MVT deposits have no general relationship with igneous activity (e.g. Leach *et al.* 2005). Some researchers have therefore indicated that the Fule deposit is not an MVT deposit (Si, 2006; Zhou *et al.* 2018*a*). The Fule deposit is located in the southern part of the NE Yunnan depression carbonate-bearing basin in the SYG area (Han *et al.* 2007*a*). The basin formed during late Sinian time and underwent tectonic uplift during Late Jurassic time (Zhang *et al.* 2005). The study of the sulphur and lead isotopes of the Fule deposit indicates that these metallogenic materials are not derived from Permian Emeishan basalts (Si, 2006; Zhou *et al.* 2018*b*), implying that the ore genesis of the deposit is not related to basalts.

As mentioned above, the most important characteristics of the Fule deposit are: (1) it is epigenetic; (2) it is hosted in the Permian dolostone (Fu *et al.* 2004; RJ Si, unpub. PhD thesis, Chinese Academy of Sciences, 2005; Yang & Xue 2012; Lü, 2014); (3) its simple mineral paragenesis (dominated by sphalerite, galena and pyrite; RJ Si, unpub. PhD thesis, Chinese Academy of Sciences, 2005; Si *et al.* 2006; ZL Li, unpub. Master thesis, University Chinese Academy of Sciences, 2016; Li *et al.* 2018*a*, *b*); (4) it is a stratiform ore body; and (5) its ore-forming fluids of 5–16 wt% NaCl equivalent at 120–210 °C (ZL Li, unpub. Master thesis, University Chinese Academy of Sciences, 2016). Interestingly, all of these features are similar to those of MVT deposits (Sangster, 1996; Leach *et al.* 2005; Leach & Taylor, 2009). Moreover, the Pb isotope ratio of sulphides (sphalerite, pyrite and galena) in the Fule deposit has been derived from metamorphic basement rocks and a small amount of lead originating from the hosted ore strata (Zhou *et al.* 2018*a*).

Combining the results of the geology and Pb and S isotopes, the Fule deposit is an MVT Pb–Zn deposit.

6. Conclusions

This study presents NanoSIMS analyses of the micromineralogy in the Fule Pb–Zn deposit, SW China. The $\delta^{34}S$ values of sulphide minerals vary from +16.1‰ to +23.0‰, exhibiting a narrow variation range and implying that the S of the Fule deposit is likely derived from the sulphates in the regional rocks (older than the Permian strata) rather than the middle Permian carbonates. Fule sulphide precipitation resulted from the mixing of a metalliferous fluid with a H_2S-rich fluid derived from the regional strata, and the S isotopic fractionation was dominated by TSR.

From the early to late mineralization stages, the $\delta^{34}S$ values of the sulphide minerals, namely, anhedral pyrite (Py1) → black-brown sphalerite (Sp2a) → brown sphalerite (Sp2b) → light yellow sphalerite (Sp2c) → subhedral–euhedral pyrite (Py2) and some single sulphide crystals, from the cores to rims, show a weak increased trend, implying that partial Rayleigh fractionation took place in the Fule deposit.

The ore genesis of the deposit is an MVT, which is not related to upper Permian Emeishan flood basalts during the mineralization process.

Acknowledgments. This research project was jointly supported by the National Natural Science Foundation of China (grant nos 41673056, 41173063), the State Key Program of National Natural Science Foundation of China (grant no. 41430315) and the National '973 Project' (grant no. 2014CB440906). We would like to thank Dr Jianchao Zhang (NanoSIMS laboratory, Beijing) for his assistance with NanoSIMS analysis, and Dr Shaohua Dong (State Key Laboratory of Ore Deposit Geochemistry, Institute of Geochemistry) for her assistance with SEM analysis.

https://doi.org/10.1017/S0016756819000852 Published online by Cambridge University Press

References

Algeo T, Shen Y, Zhang T, Lyons T, Bates S, Rowe H and Nguyen TKT (2008) Association of 34S-depleted pyrite layers with negative carbonate δ13C excursions at the Permian-Triassic boundary: evidence for upwelling of sulfidic deep-ocean water masses. *Geochemistry Geophysics Geosystems* **9**, 1–10.

Anderson GM (1983) Some geochemical aspects of sulfide precipitation in carbonate rocks. *In*: *Proceedings of International Conference on Mississippi Valley-type Lead–Zinc Deposits* (eds G Kisvarsanyi, G Sheldon, W Pratt and J Koenig), pp. 61–76. Rolla, MO: University of Missouri-Rolla.

Bai JH, Huang ZL, Zhu D, Yan ZF and Zhou JX (2013) Isotopic compositions of sulfur in the Jinshachang lead-zinc deposit, Yunnan, China, and its implication on the formation of sulfur-bearing minerals. *Acta Geologica Sinica* **87**, 1355–69.

Barker SLL, Hickey KA, Cline JS, Dipple GM, Kilburn MR, Vaughan JR and Longo AA (2009) Uncloaking invisible gold: use of NanoSIMS to evaluate gold, trace elements, and sulfur isotopes in pyrite from Carlin-type gold deposites. *Economic Geology* **104**, 897–904.

Barton PB (1967) Possible role of organic matter in the precipitation of the Mississippi Valley ores. In: *Genesis of Stratiform Lead–Zinc–Barite–Fluorite Deposits (Mississippi-Valley Type Deposits)* (ed. JS Brown), pp. 371–7. Society of *Economic Geologists, Littleton, Monograph no.* **3**.

Beard BL, Johnson CM, Skulan JL, Nealson KH, Cox L and Sun H (2003) Application of Fe isotopes to tracing the geochemical and biological cycling of Fe. *Chemical Geology* **195**, 87–117.

Canfield DE and Teske A (1996) Late Proterozoic rise in atmospheric oxygen concentration inferred from phylogenetic and sulphur-isotope studies. *Nature* **382**, 127–32.

Carr GR, Dean JA, Suppel DW and Heithersay PS (1995) Precise lead isotope fingerprinting of hydrothermal activity associated with Ordovician to Carboniferous metallogenic events in the Lachlan fold belt of New South Wales. *Economic Geology* **90**, 1467–505.

Chaussidon M, Albarède F and Sheppard SMF (1989) Sulphur isotope variations in the mantle from ion microprobe analyses of micro-sulphide inclusions. *Earth and Planetary Science Letters* **92**, 144–56.

Claypool GE, Holser WT, Kaplan IR, Sakai H and Zak I (1980) The age curves of sulfur and oxygen isotopes in marine sulfate and their mutual interpretation. *Chemical Geology* **28**(80), 199–260.

Ellis AS, Johnson TM and Bullen TD (2004) Using chromium stable isotope ratios to quantify Cr (VI) reduction: lack of sorption effects. *Environmental Science & Technology* **38**(13), 3604–7.

Fu SH, Gu XX, Wang Q, Li FY and Zhang M (2004) A preliminary study on the enrichment regularity of dispersed elements in lead-zinc deposits in the SW margin of the Yangtze platform. *Bulletin of Mineralogy, Petrology and Geochemistry* **23**, 105–8 (in Chinese with English abstract).

Gerdes G, Klenke T and Noffke N (2000) Microbial signatures in peritidal siliciclastic sediments: a catalogue. *Sedimentology* **47**, 279–308.

Habicht K, Canfield DE and Rethemeier J (1998) Sulfur isotope fractionation during bacterial reduction and disproportionation of thiosulfate and sulfite. *Geochimica et Cosmochimica Acta* **62**, 2585–95.

Haest M, Schneider J, Cloquet C, Latruwe K, Vanhaecke F and Muchez P (2010) Pb isotopic constraints on the formation of the Dikulushi Cu–Pb–Zn–Ag mineralisation, Kundelungu Plateau (Democratic Republic of Congo). *Mineralium Deposita* **45**, 393–410.

Han RS, Liu CQ, Huang ZL, Chen J, Ma DY, Lei L and Ma GS (2007a) Geological features and origin of the Huize carbonate-hosted Zn-Pb-(Ag) district, Yunnan, South China. *Ore Geology Review* **31**, 360–83.

Han RS, Zou HJ, Hu B, Hu YZ and Xun CD (2007b) Features of fluid inclusions and sources of ore-forming fluid in the Maoping carbonate-hosted Zn-Pb-(Ag-Ge) deposit, Yunnan, China. *Acta Petrologica Sinica* **23**, 2109–18 (in Chinese with English abstract).

Herrmann AM, Ritz K, Nunan N, Clode PL, Pett-Ridge J, Kilburn MR, Murphy DV, O'Donnell AG and Stockdale EA (2007) Nano-scale secondary ion mass spectrometry— a new analytical tool in biogeochemistry and soil ecology: A review article. *Soil Biology and Biochemistry* **39**, 1835–50.

Hoppe P (2006) NanoSIMS: A new tool in cosmochemistry. *Applied Surface Science* **252**, 7102–6.

Huang ZL, Chen J, Han RS, Li WB, Liu CQ, Zhang ZL, Ma DY, Gao DR and Yang HL (2004) *Geochemistry and Ore-Formation of the Huize Giant Lead–Zinc Deposit, Yunnan, Province, China: Discussion on the Relationship between the Emeishan Flood Basalts and Lead–Zinc Mineralization*. Beijing: Geological Publishing House, 1–214 pp. (in Chinese).

Huang ZL, Li XB, Zhou MF, Li WB and Jin ZG (2010) REE and C–O isotopic geochemistry of calcites from the word-class Huize Pb–Zn deposits, Yunnan, China: implication for the ore genesis. *Acta Geologica Sinica* **84**, 597–613.

Kelley KD, Wilkinson JJ, Chapman JB, Crowther HL and Weiss DJ (2009) Zinc isotopes in sphalerite from base metal deposits in the Red Dog district, northern Alaska. *Economic Geology* **104**, 767–73.

Kesler SE (1996) Appalachian Mississippi Valley-type deposits: paleoaquifers and brine provinces. *Society of Economic Geologists* **4**, 29–57.

Kiyosu Y (1980) Chemical reduction and sulfur-isotope effects of sulfate by organic matter under hydrothermal conditions. *Chemical Geology* **30**, 47–56.

Kiyosu Y and Krouse HR (1990) The role of organic acid in the abiogenic reduction of sulfate and the sulfur isotope effect. *Geochemical Journal* **24**, 21–7.

Leach DL, Macquar JC, Lagneau V, Leventhal J, Emsbo P and Premo W (2006) Precipitation of lead-zinc ores in the Mississippi Valley-type deposit at Trèves, Cévennes region of southern France. *Geofluids* **6**, 24–44.

Leach DL, Sangster DF, Kelley KD, Large RR, Garven G, Allen CR, Gutzmer J and Walters S (2005) Sediment-hosted lead-zinc deposits: a global perspective. *Economic Geology 100th Anniversary Volume*, **100**, 561–607.

Leach DL and Taylor RD (2009). Mississippi Valley-type lead-zinc deposit model. US Geological Survey, Open-File Report 2009-1213, 5 p.

Li B, Gu XC, Wen SM, Han RS, Sheng R, Xu GD, Cao Y, Wu H and Zou GF (2012) Effect of Emeishan basalt in northeast Yunnan on lead and zinc mineralization. *Mineral Resources and Geology* **26**, 95–100 (in Chinese with English abstract).

Li ZL, Ye L, Hu YS and Huang ZL (2018a) Geological significance of nickeliferous minerals in the Fule Pb–Zn deposit, Yunnan Province, China. *Acta Geochimica* **37**, 684–90.

Li ZL, Ye L, Huang ZL, Zhou JX, Hu YS and Nian HL (2018b) Mineralogical characteristics and geological significance of copper minerals in Fule Pb-Zn deposit, Yunnan Province, China. *Geological Journal of China Universities* **24**, 201–10 (in Chinese with English abstract).

Liu HC (1995) Emeishan Basalt and Pb-Zn metallogenesis. *Geology and Exploration* **4**, 1–6 (in Chinese with English abstract).

Liu HC and Lin WD (1999) *Study on the Law of Pb–Zn–Ag Ore Deposit in Northeast Yunnan, China*. Kunming: Yunnan University Press, pp. 1–468 (in Chinese).

Lü YH (2014) Lead-zinc deposits of Huize-Fule factory and typical MVT lead-zinc deposits. *Value Engineering* **16**, 309–10 (in Chinese with English abstract).

Machel HG, Krouse HR and Sassen R (1995) Products and distinguishing criteria of bacterial and thermochemical sulfate reduction. *Applied Geochemistry* **10**, 373–89.

Merce C, Carlos A and Esteve C (2004) Hydrothermal mixing, carbonate dissolution and sulfide precipitation in Mississippi Valley-type deposit. *Mineralium Deposita* **39**, 344–57.

Ohmoto H (1972) Systematics of sulfur and carbon isotopes in hydrothermal ore deposits. *Economic Geology* **67**, 551–79.

Ohmoto H, Kaiser CJ and Geer KA (1990) Systematics of sulphur isotopes in recent marine sediments and ancient sediment-hosted base metal deposits. In *Stable Isotopes and Fluid Processes in Mineralisation* (eds HK Herbert and SE Ho), pp. 70–120. Geology Department & University Extension, the University of Western Australia: Western Australia.

Ohmoto H and Rye RO (1979) Isotopes of sulfur and carbon. In *Geochemistry of Hydrothermal Ore Deposits* (ed. HL Barnes), pp. 509–567. Wiley-Blackwell, New York.

Orr WL (1974) Changes in sulfur content and isotopic ratios of sulfur during petroleum maturation–study of Big Horn Paleozoic oils. *AAPG Bulletin* **58**, 2295–318.

Peevler J, Fayek M, Misra KC and Riciputi LR (2003) Sulfur isotope microanalysis of sphalerite by SIMS: constraints on the genesis of Mississippi valley-type mineralization, from the Mascot-Jefferson City district, East Tennessee. *Journal of Geochemical Exploration* **80**, 277–96.

https://doi.org/10.1017/S0016756819000852 Published online by Cambridge University Press

Pinckey DM and Rafter TA (1972) Fractionation of sulfur isotope during ore deposition in the upper Mississipi valley zinc-lead district. *Economic Geology* **67**, 315–28.

Pósfai M, Cziner K, Márton E, Márton P, Buseck PR, Frankel RB and Bazylinski DA (2001) Crystal-size distributions and possible biogenic origin of Fe sulfides. *European Journal of Mineralogy* **13**, 691–703.

Ren SL, Li YH, Zeng PS, Qiu WL, Fan CF and Hu GY (2018) Effect of sulfate evaporate salt layer in mineralization of the Huize and Maoping lead-Zinc deposits in Yunnan: Evidence from sulfur isotope. *Acta Geologica Sinica* **92**, 1041–55 (in Chinese with English abstract).

Sakai H (1968) Isotopic properties of sulfur compounds in hydrothermal processes. *Geochemical Journal* **2**, 29–49.

Sangster DF (1996) Mississippi Valley-type lead-zinc. In *Geology of Canadian Mineral Deposit Types* (eds OR Eckstrand, WD Sinclair and RI Thorpe), pp. 253–61. Geological Society of America, vol.**8**.

Seal RRI (2006) Sulfur isotope geochemistry of sulfide minerals. *Reviews in Mineralogy and Geochemistry* **61**, 633–77.

Shentu LY, Han RS, Li B and Qiu WL (2011) Study on the isotope geochemistry of the Maoping Pb-Zn deposit, Zhaotong, Yunnan. *Mineral Resources and Geology* **25**, 211–6 (in Chinese with English abstract).

Si RJ, Gu XX, Pang XC, Fu SH and Li FY (2006) Geochemical character of dispersed element in sphalerite from Fule Pb-Zn polymetal deposit, Yunnan Province. *Kuangwu Yanshi* **26**, 75–80 (in Chinese with English abstract).

Tang YY, Bi XW, Fayek M, Hu RZ, Wu LY, Zou ZC, Feng CX and Wang XS (2014) Microscale sulfur isotopic compositions of sulfide minerals from the Jinding Zn–Pb deposit, Yunnan Province, Southwest China. *Gondwana Research* **26**, 594–607.

Tang YY, Bi XW, He LP, Wu LY, Feng CX, Zou ZC, Tao Y and Hu RZ (2011) Geochemical characteristics of trace elements, fluid inclusions and carbon–oxygen isotopes of calcites in the Jinding Zn–Pb deposit, Lanping, China. *Acta Petrologica Sinica* **27**, 2635–45 (in Chinese with English abstract).

Tu GZ (1984) *Geochemistry of Strata-bound Ore Deposits in China*, Vol. **I**, Beijing: Science Press, pp. 13–69 (in Chinese).

Wacey D, Kilburn MR, Saunders M, Cliff J and Brasier MD (2011) Microfossils of sulphur-metabolizing cells in 3.4-billion-year-old rocks of Western Australia. *Nature Geoscience* **4**, 698–702.

Wei AY, Xue CD, Xiang K, Li J, Liao C and Akhter QJ (2015) The ore-forming process of the Maoping Pb–Zn deposit, Northeastern Yunnan, China: Constraints from cathodoluminescence (CL) petrography of hydrothermal dolomite. *Ore Geology Reviews* **70**, 562–77.

Winterholler B, Hoppe P, Andreae MO and Foley S (2006) Measurement of sulfur isotope ratios in micrometer-sized samples by NanoSIMS. *Applied Surface Science* **252**, 7128–31.

Worden RH, Smalley PC and Oxtoby NH (1995) Gas souring by the thermochemical sulfate reduction at 140°C. *AAPG Bulletin* **79**, 854–63.

Wu Y, Zhang CQ, Mao JW, Ouyang HG and Sun J (2013) The genetic relationship between hydrocarbon systems and Mississippi Valley-type Zn–Pb deposits along the SW margin of Sichuan Basin, China. *International Geology Review* **55**, 941–57.

Xie JR (1963) Problems pertaining to geology and ore deposits of a copper deposit in Shansi province. *Science China Mathematics* **6**, 1345–55.

Xiong SF, Gong YJ, Jiang SY, Zhang XJ, Li Q and Zeng GP (2018) Ore genesis of the Wusihe carbonate-hosted Zn-Pb deposit in the Dadu River Valley district, Yangtze Block, SW China: evidence from ore geology, S-Pb isotopes, and sphalerite Rb-Sr dating. *Mineralium Deposita* **53**, 967–79.

Xue CJ, Chi GX and Fayek M (2015) Micro-textures and in situ sulfur isotopic analysis of spheroidal and zonal sulfides in the giant Jinding Zn-Pb deposit, Yunnan, China: Implications for biogenic processes. *Journal of Asian Earth Sciences* **103**, 288–304.

Yang N and Xue BG (2012) A study on the metallogenetic rule of Pb-Zn deposit concentration area in the Yunnan. *Yunnan Geology* **1**, 1–11 (in Chinese with English abstract).

Yang W, Hu S, Zhang JC, Hao JL and Lin YT (2015) NanoSIMS analytical technique and its applications in earth sciences. *Science China Earth Sciences* **58**, 1758–67 (in Chinese with English abstract).

Ye L, Li ZL, Hu YS, Huang ZL, Zhou JX, Fan HF and Danyushevskiy L (2016) Trace elements in sulfide from the Tianbaoshan Pb-Zn deposit, Sichuan Province, China: A LA-ICPMS study. *Acta Petrologica Sinica* **32**, 3377–93.

Yuan B, Mao JW, Yan XH, Wu Y, Zhang F and Zhao LL (2014) Sources of metallogenic materials and metallogenic mechanism of Daliangzi Ore Field in Sichuan Province: Constraints from geochemistry of S, C, H, O, Sr isotope and trace element in sphalerite. *Acta Petrologica Sinica* **30**, 209–20 (in Chinese with English abstract).

Zhang CQ, Mao JW, Wu SP, Li HM, Liu F, Guo BJ and Gao DR (2005) Distribution, characteristics and genesis of Mississippi Valley-type lead-zinc deposits in Sichuan-Yunnan-Guizhou area. *Mineral Deposits* **24**, 336–48 (in Chinese with English abstract).

Zhang CQ, Wu Y, Hou L and Mao JW (2015) Geodynamic setting of mineralization of Mississippi Valley-type deposits in world-class Sichuan-Yunnan-Guizhou Zn-Pb triangle, southwest China: Implications from age-dating studies in the past decade and the Sm-Nd age of Jinshachang deposit. *Journal of Asian Earth Sciences* **103**, 103–14.

Zhang JC, Lin YT, Yang W, Shen WJ, Hao JL, Hu S and Cao MJ (2014) Improved precision and spatial resolution of sulfur isotope analysis using Nanosims. *Journal of Analytical Atomic Spectrometry* **29**, 1934–43.

Zhao Z (1995) Metallogenic model of Pb-Zn deposits in northeastern Yunnan. *Journal of Yunnan Geology* **14**, 350–4 (in Chinese with English abstract).

Zheng MH and Wang XC (1991) Genesis of the Dalinagzi Pb-Zn deposit in Sichuan, China. *Economic Geology* **86**, 831–46.

Zhong KH, Liao W, Song MY and Zhang YQ (2013) Discussion on sulfur isotope of Huize Pb-Zn deposit in Yunnan, China. *Journal of Chengdu University of Technology (Science and Technology Edition)* **40**, 130–8 (in Chinese with English abstract).

Zhou CX, Wei CS and Guo JY (2001) The source of metals in the Qilingchang Pb–Zn deposit, Northeastern Yunnan, China: Pb–Sr isotope constraints. *Economic Geology* **96**, 583–98.

Zhou JX, Huang ZL, Bao GP and Gao JG (2013a). Sources and thermo-chemical sulfate reduction for reduced sulfur in the hydrothermal fluids, southeastern SYG Pb-Zn metallogenic province, SW China. *Journal of Earth Science* **24**, 759–71.

Zhou JX, Huang ZL, Gao JG and Wang T (2012) Sources of ore-forming metals and fluids, and mechanism of mineralization, Maozu large carbonare-hosted Lead-Zinc deposit, Northeast Yunnan Province. *Journal of Mineralogical and Petrological Sciences* **32**, 62–9 (in Chinese with English abstract).

Zhou JX, Huang ZL, Gao JG and Yan ZF (2013b) Geological and C–O–S–Pb–Sr isotopic constraints on the origin of the Qingshan carbonate-hosted Pb-Zn deposit, Southwest China. *International Geology Review* **55**, 904–16.

Zhou JX, Huang ZL, Zhou GF, Li XB, Ding W and Bao GP (2010) Sulfur isotopic composition of the Tianqiao Pb-Zn ore deposit, Northwest Guizhou Province, China: Implications for the source of sulfur in the ore-forming fluids. *Chinese Journal of Geochemistry* **29**, 301–6.

Zhou JX, Huang ZL, Zhou MF, Li XB and Jin ZG (2013c) Constraints of C–O–S–Pb isotope compositions and Rb–Sr isotopic age on the origin of the Tianqiao carbonate-hosted Pb–Zn deposit, SW China. *Ore Geology Reviews* **53**, 77–92.

Zhou JX, Luo K, Wang XC, Wilde SA, Wu T, Huang ZL, Cui YL and Zhao JX (2018a) Ore genesis of the Fule Pb-Zn deposit and its relationship with the Emeishan Large Igneous Province: Evidence from mineralogy, bulk C-O-S and in situ S-Pb isotopes. *Gondwana Research* **54**, 161–79.

Zhou JX, Wang XC, Wilde SA, Luo K, Huang Z L, Wu T and Jin ZG (2018b) New insights into the metallogeny of MVT Zn-Pb deposits: A case study from the Nayongzhi in South China, using field data, fluid compositions, and in situ S-Pb isotopes. *American Mineralogist* **103**, 91–108.

Zhou JX, Xiang ZZ, Zhou MF, Feng YX, Luo K, Huang ZL and Wu T (2018c) The giant Upper Yangtze Pb–Zn province in SW China: Reviews, new advances and a new genetic model. *Journal of Asian Earth Sciences* **154**, 280–315.

Zhu CW, Wen HJ, Zhang YX, Fu SH, Fan HF and Cloquet C (2017) Cadmium isotope fractionation in the Fule Mississippi Valley-type deposit, southwest China. *Mineralium Deposita* **52**, 675–86.

https://doi.org/10.1017/S0016756819000852 Published online by Cambridge University Press